



Facile Synthesis of Monodispersed α -Ni(OH)₂ Microspheres Assembled by Ultrathin Nanosheets and Its Performance for Oxygen Evolution Reduction

Juan Yu, Shencheng Pan, Yongxing Zhang, Qinzhuang Liu and Bing Li*

Department of Materials Science and Engineering, Huaibei Normal University, Huaibei, China

OPEN ACCESS

Edited by:

Xingang Ren,
Anhui University, China

Reviewed by:

Fei Ye,
The University of Hong Kong,
Hong Kong
Hong Zhang,
École Polytechnique Fédérale de
Lausanne, Switzerland

*Correspondence:

Bing Li
bingli@mail.usc.edu.cn

Specialty section:

This article was submitted to
Energy Materials,
a section of the journal
Frontiers in Materials

Received: 12 March 2019

Accepted: 14 May 2019

Published: 04 June 2019

Citation:

Yu J, Pan S, Zhang Y, Liu Q and Li B
(2019) Facile Synthesis of
Monodispersed α -Ni(OH)₂
Microspheres Assembled by Ultrathin
Nanosheets and Its Performance for
Oxygen Evolution Reduction.
Front. Mater. 6:124.
doi: 10.3389/fmats.2019.00124

Electrocatalytic water splitting is an efficient route to generate renewable energy sources, in which the noble metal materials are usually used as electrocatalysts. But the high price and scarcity of these catalysts impede their large-scale applications. Ni-based materials are considered to be the most suitable catalytic materials to substitute these noble metal materials. In this paper, the monodispersed α -Ni(OH)₂ microspheres assembled by ultrathin nanosheets were synthesized by a facile solvothermal method. This method was surfactant-free and no precipitator was used. The as-obtained products were well-characterized by X-ray diffraction (XRD), field emission scanning electron microscope (FESEM), transmission electron microscope (TEM), thermal gravimetric (TG) analysis, and X-ray photoelectron spectroscopy (XPS). The results of N₂ adsorption/desorption isotherm indicate that the BET surface area of the products was 169.94 m²g⁻¹, and the pore-size distribution centered at 3.5 nm. Then, the electrochemical properties were evaluated by linear sweep voltammetry (LSV) in 1 M KOH. At a current density of 10 mA cm², the overpotential for the α -Ni(OH)₂-MS is 320 mV, and the Tafel slope is 98.7 mV dec⁻¹, indicating its excellent reaction kinetics for an efficient catalyst toward oxygen evolution reaction (OER).

Keywords: α -Ni(OH)₂, solvothermal, ultrathin nanosheets, water splitting, oxygen evolution reaction, electrocatalysis

INTRODUCTION

The depletion of fossil energy has caused many serious environmental problems, such as air pollution and greenhouse effect (Dou et al., 2016; Tahir et al., 2017). Therefore, the exploitation of environment-friendly renewable energy is very crucial to resolve this global energy predicament (Alarawi et al., 2019; Sun et al., 2019; Wang et al., 2019). Hydrogen, as a clean and pollution-free energy, is considered to be the most promising alternative energy resource (Midilli and Dincer, 2008; McCrory et al., 2015; Du et al., 2018; Xie et al., 2018). To date, electrocatalytic and photocatalytic water splitting are two main methods for hydrogen production (Wang J. et al., 2016; Roger et al., 2017; Kim et al., 2018; Kadi and Mohamed, 2019). Considering the low efficiency of photocatalytic water splitting, electrocatalytic water splitting possesses its advantage to produce hydrogen.

As is well-known, the electrocatalytic water splitting includes two half reactions, the oxygen evolution reaction (OER) at anode and the hydrogen evolution reaction (HER) at cathode (Yang et al., 2015; Masa et al., 2016; Guo et al., 2017; Suen et al., 2017; Rakov et al., 2018). However, water splitting for hydrogen generation is mainly limited by the OER, because it is a multi-step proton-coupled electron transfer process, which needs a high overpotential to overcome the large energy barrier (Man et al., 2011). At present, the noble metal-based materials, such as IrO₂ and RuO₂, are the commonly used electrocatalysts for OER. But the high price and scarcity of these catalysts impede their large-scale applications (Petrykin et al., 2010; Reier et al., 2012; McCrory et al., 2013).

Recently, the first-row transition catalysts, such as Ni-, Fe-, Co-, Cu-, Mn-based materials, have been used to be the possible alternatives, not only because of their abundant reserves in the earth but also their inexpensive nature compared with the novel metals (Du and Eisenberg, 2012; Gong et al., 2013; Dou et al., 2016; Wang J. et al., 2016; Krehula et al., 2018; Liu et al., 2019). The previous reports have pointed out that Ni-based materials have a large potential as the OER catalysts for water splitting and are regarded as one type of excellent electrocatalysts (Subbaraman et al., 2012). In general, there are several strategies to improve the OER activity of Ni-based catalysts. The first strategy is to introduce other elements to form multi-metallic materials, such as Ni-Co (Zhao et al., 2014; Liu et al., 2015; Peng et al., 2015; Wang H. et al., 2015; Li et al., 2016), Ni-Fe (Gong et al., 2013; Qiu et al., 2014; Gong and Dai, 2015; Ma et al., 2015; Yu et al., 2015; Jia et al., 2017), Ni-Mn (Cordoba et al., 1986; Menezes et al., 2015; Sumboja et al., 2017), Ni-Co-Fe (Yan et al., 2017), and so on, in which the coordination of different elements could provide more oxidation states as well as redox active sites. Some of these Ni-based materials have been employed as bifunctional catalysts for the OER and ORR in alkaline medium. But, in these materials, there is a difficulty to control the repeatability and the ratio of elements. The second one is to prepare metal decorated Ni-based materials or design a composite structure (Jia et al., 2017; Sun et al., 2019; Zhai et al., 2019). The third one is to synthesis Ni-based sulfides, phosphides, and selenides materials, such as Ni-S, Ni-P, and Ni-Se, which have also been reported as efficient electrocatalysts for OER (Anantharaj et al., 2016; Dong et al., 2016; Wang M. et al., 2016; Li et al., 2017; Chen et al., 2018). But, as we all know, the processes of decoration, sulfuration, or phosphorization are complicated and sensitive to the temperature and treating time. Another strategy is to control the morphologies through the changes of solvents, surfactants, reaction conditions, and preparation methods, *etc.* (Ouyang et al., 2015; Qi et al., 2015; Shi and Zhang, 2016). Among these Ni-based materials, Ni(OH)₂ OER catalysts with various morphologies have been used as the promising electrochemical materials (Aghazadeh et al., 2011; Lee et al., 2011b; Anantharaj et al., 2017). Ni(OH)₂ has two phases: α - and β -Ni(OH)₂. It is environmentally friendly and inexpensive. Gao et al. (2014) prepared hollow sphered α -Ni(OH)₂ nanoparticles by a solvothermal route with oleylamine as surfactant, and found that the α -Ni(OH)₂ nanoparticles displayed superior OER activity to the β -Ni(OH)₂ nanoplates. Then, (Stern and

Hu, 2014) synthesized β -Ni(OH)₂ nanoparticles with different morphologies by a coprecipitation method using NaOH as a precipitator and realized a lower overpotential of 300 mV. In addition, Niu et al. (2017) grew β -Ni(OH)₂ nanoplate array directly on NiAl foil and the resulting Ni(OH)₂/NiAl electrode showed higher OER electrocatalytic activity. In comparison to β -Ni(OH)₂, α -Ni(OH)₂ catalysts demonstrate higher activity during OER, ascribed to their large interlayer spaces and unique redox characteristics. Moreover, α -Ni(OH)₂ transforms to γ -NiOOH in the electrochemical process, and the α -Ni(OH)₂/ γ -NiOOH pairs can deliver more electrons than β -Ni(OH)₂/ β -NiOOH (Tong et al., 2012). Therefore, the α -Ni(OH)₂ usually shows better electrochemical performance than β -Ni(OH)₂. Although there are some reports on the use of Ni(OH)₂ catalysts with varied morphologies via different synthesis methods for the OER, the related research on the α -Ni(OH)₂ are comparatively weak. Usually, urea is widely used as precipitator to synthesis α -Ni(OH)₂ because of its relatively mild hydrolytic process, which can provide an alkaline environment and is favorable to formation of product (Jeevanandam et al., 2001; Yan et al., 2012; Wang Q. et al., 2015; Wang D. et al., 2018). But, it is still a challenge to develop a facile one-step, low-cost and mild route for the synthesis of α -Ni(OH)₂ without using urea as precipitator.

In this paper, the monodispersed α -Ni(OH)₂ microspheres assembled by ultrathin nanosheets were synthesized by a facile solvothermal method. This method was surfactant-free and no precipitator was used, such as urea, indicating an efficient and low-cost process. The as-obtained products were well-characterized by x-ray diffraction (XRD), field emission scanning electron microscope (FESEM), and transmission electron microscope (TEM). The LSV test shows a small overpotential of 320 mV at the current density of 10 mA cm⁻² with a smaller Tafel slope of 98.7 mV dec⁻¹. This study presents a simple and economical method to synthesize high performance non-noble electrocatalysts for OER and thus is significant for the development of water splitting.

EXPERIMENTAL SECTION

Synthesis of α -Ni(OH)₂

All chemicals were of analytical grade and used without any further purification. The α -Ni(OH)₂ was synthesized by a simple solvothermal method. In a typical synthesis case, 0.2377 g of NiCl₂·6H₂O was dissolved in mixed solvents of 30 ml alcohol and 10 ml ethylene glycol (EG) and stirred for 30 min at room temperature. Then, the resulting solution was transferred into a 100 ml Teflon-lined stainless steel autoclave. The autoclave was sealed and heated at 170°C for 24 h. After the autoclave cooled down to room temperature naturally, the Ni(OH)₂ suspension was centrifuged and washed with deionized water and alcohol several times. Finally, the obtained Ni(OH)₂ was dried in a vacuum oven at 60°C overnight. Hereinafter, we call this mixed solvothermal synthesized Ni(OH)₂ as α -Ni(OH)₂-MS. For comparison, we also synthesized another sample with only EG as the solvent, which was denoted as α -Ni(OH)₂-EG.

Characterization

Powder x-ray diffraction (XRD) patterns of the samples were obtained with a PANalytical Empyrean x-ray diffractometer in the diffraction 2θ angle range from 5 to 80° using Cu $K\alpha$ radiation ($\lambda = 1.5418 \text{ \AA}$). Field emission scanning electron microscopy (FESEM, JEOLJSM-S4800) and transmission electron microscopy (TEM, JEM-2100) were used to characterize the morphologies of the sample. The X-ray energy dispersive spectroscopy (EDS) and EDS elemental mapping were performed with an EDS detector equipped in the JEM-2100 TEM. The surface elemental information was determined by high-resolution X-ray photoelectron spectroscopy (XPS, ESCALAB-250Xi, Thermo Fisher Scientific) with monochromatic Al-anode x-ray source (Al $K\alpha$ $h\nu = 1486.6 \text{ eV}$). The specific surface area and the pore size distribution of samples were obtained from a N₂ adsorption/desorption analysis performed at 77 K on a Micromeritics TriStar II 3020 system. The specific surface area was calculated by the Barrett-Joyner-Halenda (BJH) method, and the pore size distribution was obtained from the adsorption branch of the isotherms by the BJH method. The wetting property of the samples was investigated by water contact angle measurement (JC2000C1, Zhongchen Instrument).

Electrochemical Measurements

All the electrochemical measurements were performed on a CHI-760E electrochemical workstation using a standard three-electrode system, with the Ni(OH)₂ catalysis loaded on the Ni foam (NF) as the working electrode, a Pt foil as the counter electrode, and Ag/AgCl electrode as reference electrode. The working electrode was prepared as follows. The NF with a size of 2 cm × 1 cm × 1 mm was initially soaked with 3M HCL solution in an ultrasonic bath for 30 min to remove impurities and oxide layer adhered to it. Then, it was washed by deionized water and ethanol. Finally, it was dried several hours at 60°C under vacuum. Three milligram Ni(OH)₂ was ultrasonically dispersed into the mixture of 1 mL ethanol and Nafion (0.5 wt.%, 30 μL) to form a homogeneous ink, which was then dropped onto the above NF by pipette. The typical catalyst loading amount was about 0.3 mg cm⁻². During electrochemical test, 1M KOH (pH = 13.6) solution was employed as the electrolyte. All potentials measured were calibrated to the reversible hydrogen electrode (RHE) scale by the relationship: $E_{\text{RHE}} = E_{\text{Ag/AgCl}} + 0.197 + 0.059 \times \text{pH}$. Before the experiments, all the electrodes were cycled at a scan rate of 50 mV s⁻¹ until stable cyclic voltammetry (CV) profiles were recorded. The LSV curves of the samples were recorded at a scan rate of 5 mV s⁻¹. Electrochemical impedance spectra (EIS)

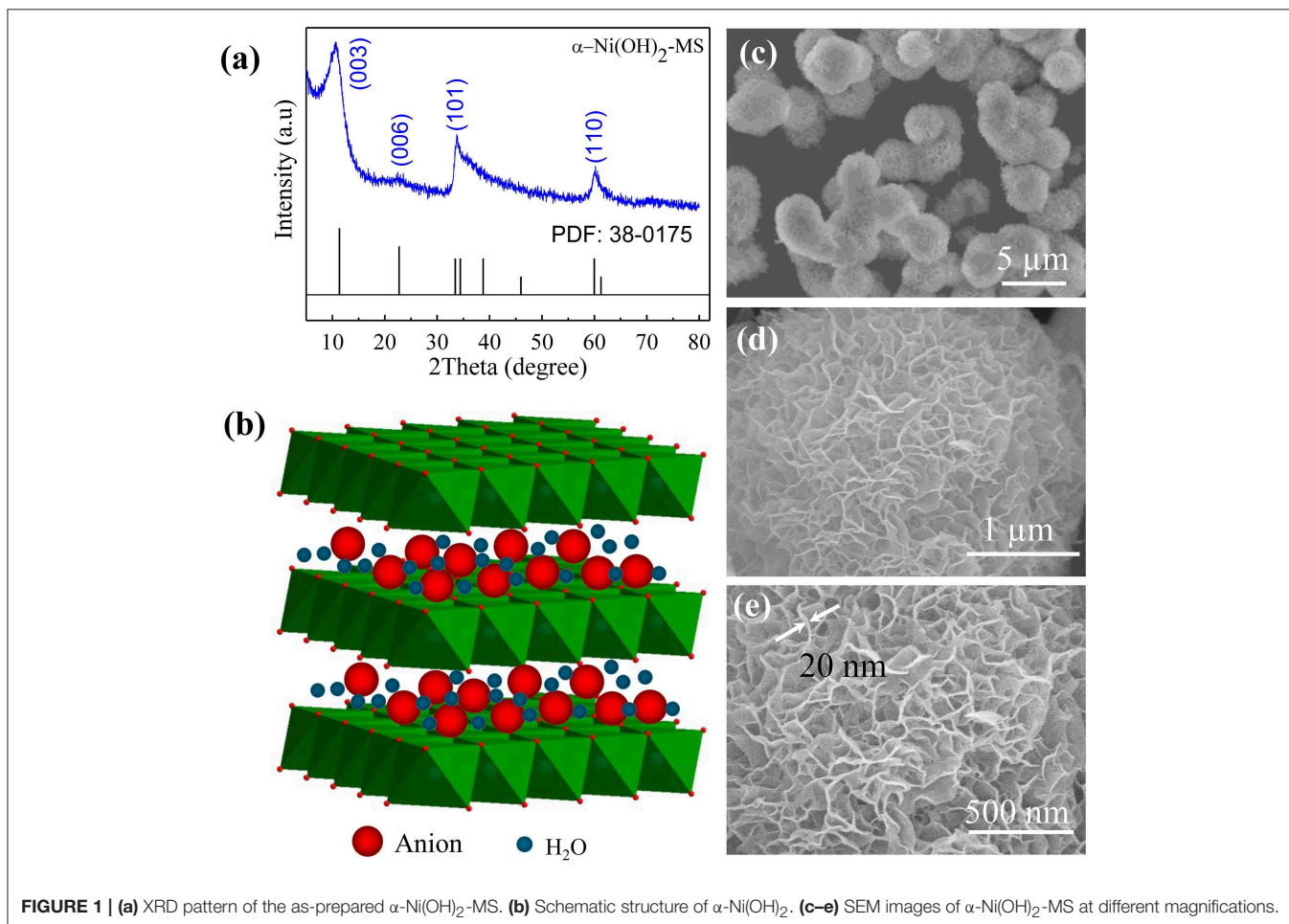


FIGURE 1 | (a) XRD pattern of the as-prepared α -Ni(OH)₂-MS. (b) Schematic structure of α -Ni(OH)₂. (c-e) SEM images of α -Ni(OH)₂-MS at different magnifications.

measurements were carried out at 0.5 V (vs. RHE) from 100 kHz to 0.01 Hz. All data were obtained without *iR*-compensation.

RESULTS AND DISCUSSION

Figure 1a shows the XRD pattern of the synthesized α -Ni(OH)₂-MS product. All the reflection peaks in the XRD pattern can be indexed to rhombohedral α -Ni(OH)₂ (JCPDS No. 38-0175, α -Ni(OH)₂·0.75H₂O). The four characteristic peaks located at 10.73, 22.87, 33.85, and 60.21° correspond to the (003), (006), (101), and (110) diffraction planes, respectively. As we all know, α -Ni(OH)₂ has a hydrotalcite-like structure comprised

of random stacked Ni(OH)₂ layers along the *c*-axis intercalated with water and/or anion, as shown in **Figure 1b**. The asymmetric diffraction peak appearing in the 2 θ range of 33.5–34.5° is characteristic of the turbostratic disorder in the α -Ni(OH)₂ layered structures. This phenomenon can be explained by that the hydrotalcite-like layers Ni(OH)₂ stacked along the *c*-axis that randomly twist to each other. This turbostratic disorder has also been observed in many other α -Ni(OH)₂ samples (Cheng and Hwang, 2009; Lee et al., 2011b). Noteworthily, compared with the standard PDF card, all corresponding peaks move to the lower angle side slightly, suggesting an increase of the *d* spacing along the *c*-axis, because the basal spacing can be altered by changing the species and quantities intercalated in the interlayer galleries.

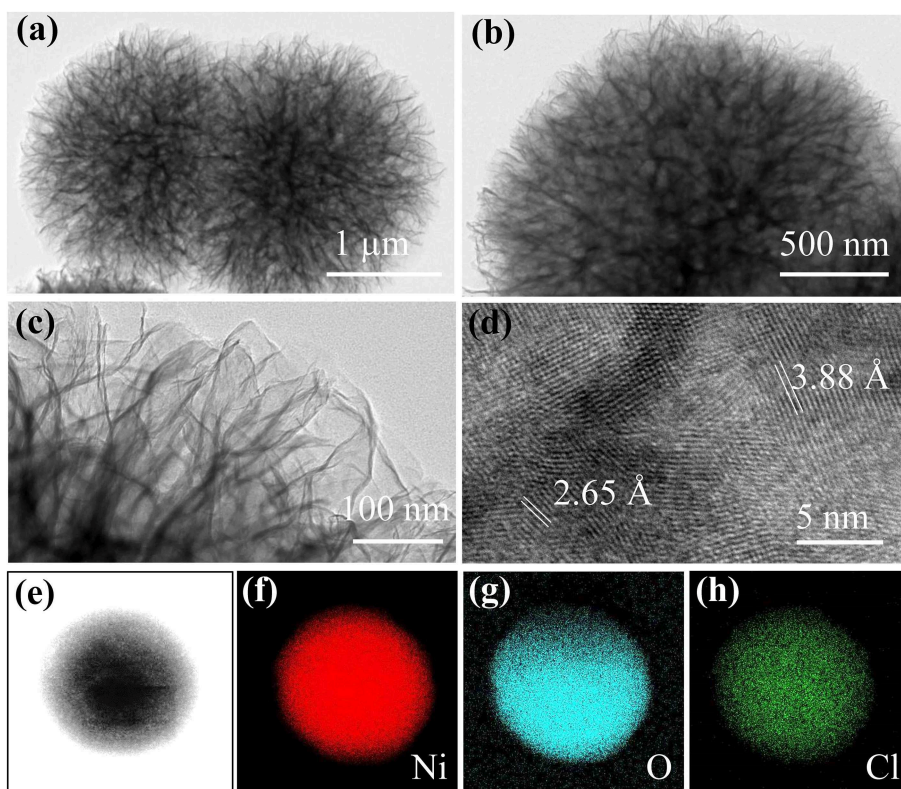


FIGURE 2 | (a–c) TEM images of α -Ni(OH)₂-MS at different magnifications. (d) HRTEM image. (f–h) EDS mapping of Ni, O, and Cl in the area of (e).

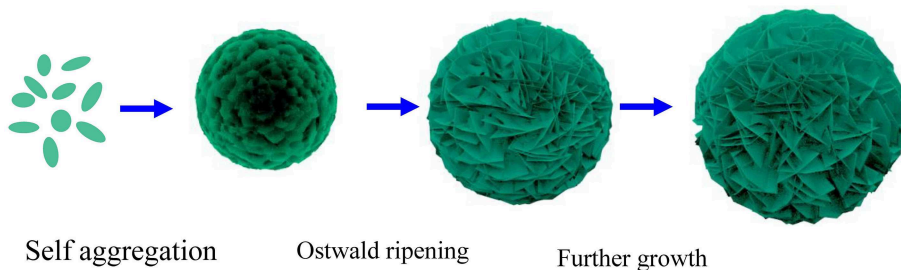


FIGURE 3 | Schematic illustration for the synthesis of α -Ni(OH)₂-MS.

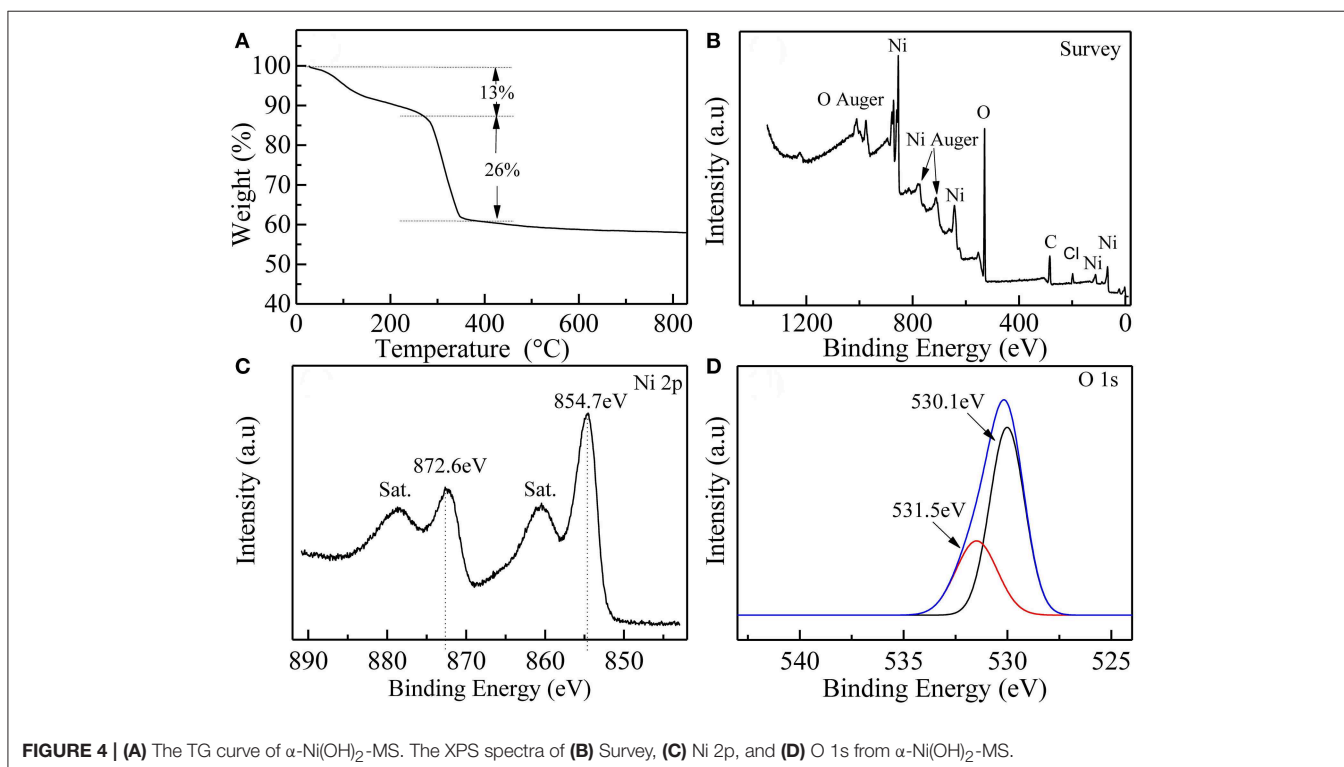
In our case, these shifts are related to the different composition, i.e., the different amount of water molecules and the presence of Cl⁻ ions in our sample. Moreover, the broad diffraction peaks can also be ascribed to the inhomogeneous distribution of Cl⁻ ions and water molecules in the layered structure. The morphology and structure of α -Ni(OH)₂-MS composite were characterized by FESEM. **Figure 1c** clearly shows that the sample is composed of many monodispersed microspheres with a diameter of several μ m. The surface is not smooth and many flakes can be seen, as shown in **Figure 1d**. A high-magnification SEM micrograph, as shown in **Figure 1e**, illustrates that these spheres are assembled by many uniform curly nanosheets. These nanosheets with a thickness of about 20 nm, as shown by the white arrows in **Figure 1e**, were connected to each other to form the 3D microsphere hierarchical structure.

Figures 2a–c shows TEM images of α -Ni(OH)₂-MS at different magnifications. Hierarchical morphology was clearly observed, which was well-matched with the SEM images. The spheres seem to be composed of many nanowires at first sight, as shown in **Figures 2a,b**. But, after careful observation, we realize that it is just the edges of the ultrathin nanosheets parallel to our sight line. The high magnification TEM image further confirms that numerous, very thin nanosheet structures with irregular shapes gathered and formed the hierarchical spheres. In **Figure 2d**, the lattice fringes were determined to be 3.88 and 2.65 Å, which match the spaces of the (006) and (101) planes of the hydroxalite-like structure, respectively. Element mappings of the α -Ni(OH)₂-MS in the area of **Figure 2e** are displayed in **Figures 2f–h**. The images are captured by recording the intensity

and distribution of characteristic X-ray. The three different colored areas shown in **Figures 2f–h** indicate the distribution of Ni, O, and Cl, respectively. The appearance of Cl can be ascribed to the intercalated Cl⁻ ions in the layered structure.

To further confirm the surface properties of α -Ni(OH)₂-MS microsphere, the sample was examined by Fourier transform infrared (FTIR) spectroscopy in the range of 400–4,000 cm⁻¹ and the result is shown in **Figure S1**. The typically broad band around 3,406 cm⁻¹ corresponds to the O–H stretching vibration of the hydrogen-bonded hydroxyl groups and interlayered water molecules located in the brucite-like layer (Wang Q. et al., 2015). The band around 1,627 cm⁻¹ can be assigned to the bending mode of the interlayered water molecules (Yan et al., 2012; Wang Q. et al., 2015). The absorption bands located at 1,384 and 1,091 cm⁻¹ are attributed to the characteristic absorption peaks of carbonate ions derived from the atmospheric CO₂, as reported previously (Liu et al., 2005; Li et al., 2013). The band located at around 669 cm⁻¹ in the low wavenumber regions is ascribed to the δ_{OH} vibration (Yan et al., 2012; Wang Q. et al., 2015).

In order to observe the evolution progress of the α -Ni(OH)₂-MS spheres, time dependent experiments were carried out, as shown in **Figure S2**. At the initial stage, some lamellas are formed and then assembled into solid construction 3D microspheres, in order to minimize surface free energy. With the extension of reaction time and the decrease of reactant concentration in the solution, due to the mass diffusion and Ostwald ripening, these lamellas on the microspheres become thinner and thinner. Then, with the further extension of reaction time, the 3D hierarchical α -Ni(OH)₂ microspheres assembled by ultrathin nanosheets



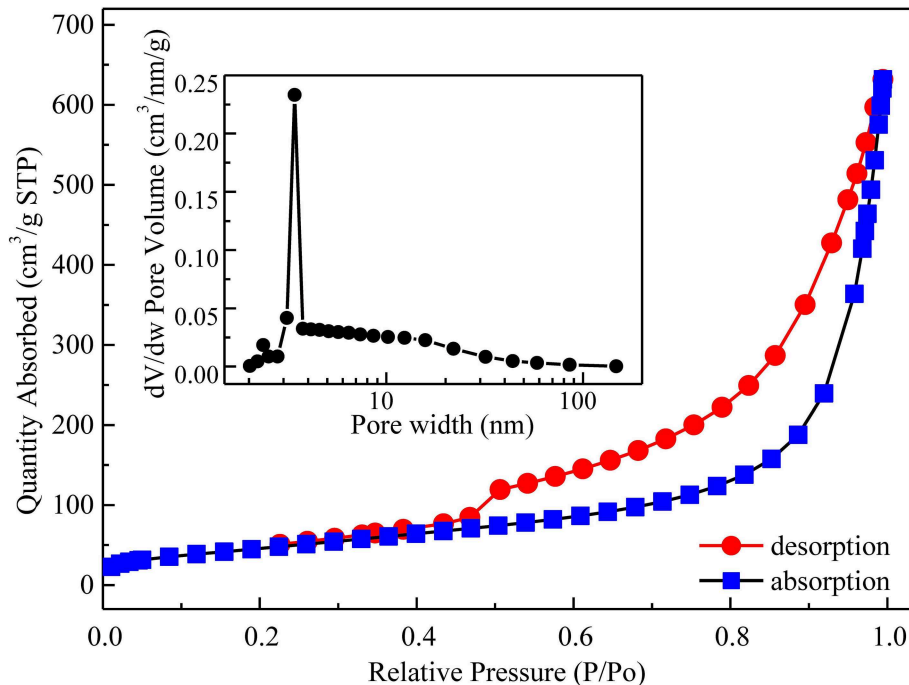


FIGURE 5 | N₂ adsorption/desorption isotherms of α -Ni(OH)₂-MS. The inset shows pore-size distributions.

TABLE 1 | Previously reported BET specific surface areas of Ni(OH)₂.

Materials	BET (m ² g ⁻¹)	Ref.
α -Ni(OH) ₂ microspheres	169.94	This work
Flower-like Co-doped Ni(OH) ₂	94	Wang Q. et al., 2015
α -Ni(OH) ₂ microspheres	101.3	Wang D. et al., 2018
α -Ni(OH) ₂ hollow spheres	57.82	Gao et al., 2014
β -Ni(OH) ₂ nanoplates	35.84	Gao et al., 2014
β -Ni(OH) ₂ nanoparticles	51.95	Gao et al., 2014
β -Ni(OH) ₂ microspheres	40.45	Du et al., 2016
β -Ni(OH) ₂ /GO	53.9	Zhai et al., 2019

are formed with regular morphologies. Based on the analysis mentioned above, a self-assembly formation mechanism of the hierarchical α -Ni(OH)₂-MS spheres is presented in **Figure 3**.

There are two obvious weight loss regions in the thermal gravimetric (TG) analysis curve of the α -Ni(OH)₂-MS, which can be observed in **Figure 4A**. Below 270°C, the 13% weight loss is induced by the removal of adsorbed water and intercalated water molecules. In the temperature region of 270–400°C, the weight loss reaches about 26%, which can be ascribed to the decomposition of Ni(OH)₂ to NiO. Here, the TG analysis further proves the presence of adsorbed and intercalated water molecules, indicating the product is α -phase Ni(OH)₂. The result is consistent with references (Lee et al., 2011a; Tian et al., 2012; Aghazadeh et al., 2014). XPS analysis was also performed to verify the elemental compositions and chemical valences of the sample, as shown in **Figures 4B–D**. In **Figure 4B**, the survey spectrum

shows obvious peaks from the elements of Ni, O, and Cl. In the high-resolution Ni 2p spectrum (**Figure 4C**), the Ni 2p_{3/2} (854.7 eV) and Ni 2p_{1/2} (872.6 eV) peaks, accompanied with two shakeup satellites (denoted as “Sat.”), indicate the presence of Ni²⁺ in the sample (Anantharaj et al., 2017; Liu et al., 2017). As shown in **Figure 4D**, the O 1s spectrum can be well-fitted using two peaks. The peak at 531.5 eV is assigned to O 1s electrons from OH⁻, and the other peak at 530.1 eV represents physically adsorbed H₂O (Anantharaj et al., 2017; Zhou et al., 2018).

The specific surface area and pore size distribution measurements were determined by Barrett-Joyner-Halenda (BJH) analysis. **Figure 5** shows N₂ adsorption/desorption isotherms and the inset gives corresponding BJH pore size distribution curves of the α -Ni(OH)₂-MS. Obviously, the sample displays type IV N₂ adsorption/desorption isotherms with an obvious H3 type hysteresis loop at the relative pressure (P/P₀) range between 0.5 and 1.0, according to Brunauer-Deming-Deming-Teller (BDDT) classification, which reveals its mesoporous characteristic. From the isotherms, the Brunauer-Emmett-Teller (BET) specific surface area of the α -Ni(OH)₂-MS is calculated to be 169.94 m²g⁻¹. The pore size distribution (the inset in **Figure 5**) obtained from the adsorption branch of the isotherms by the BJH method further confirms a mesopores structure within a size range of 2–20 nm centered at 3.5 nm. The large mesoporous structure is the result of interstitial space between the nanosheets. Moreover, the large value of absorbed N₂ at the range of p/p₀ 0.9–1.0 implies the presence of amounts of macropores, which are derived from the interparticle distance between the Ni(OH)₂ microspheres. Such a macro/mesoporous

structure is of benefit to the adsorption of electrolyte ions, accelerates the transfer of electrolyte ions, and provides more electroactive sites, thus enhances the electrochemical activity.

Many previous works indicate that the morphologies and BET surface areas play an important role in the electrochemical activity. Many efforts have been made to prepare catalysts with different morphologies and BET surface areas. In our case, the highly monodispersed α -Ni(OH)₂ microspheres assembled by ultrathin nanosheets were synthesized by a template- and surfactant-free method. Interestingly, no precipitator was used and the morphologies can be easily tuned by the ratio of alcohol and EG in the solvents. For comparison, we also synthesized another sample with only EG as the solvent, which was denoted as α -Ni(OH)₂-EG. **Figure S3** shows the XRD pattern of this product. It can also be indexed to rhombohedral α -Ni(OH)₂. The corresponding TEM images were shown in **Figure S4**, in which we can see that the products were also composed of flakes. But the thickness of the flakes were larger than that of the α -Ni(OH)₂-MS. **Figure S5** shows N₂ adsorption/desorption isotherms and corresponding BJH pore size distribution curves of

the α -Ni(OH)₂-EG. The BET specific surface area of this sample is determined to be 72.31 m²g⁻¹, which is about half of that for the α -Ni(OH)₂-MS. The BET specific surface areas are also compared with other Ni(OH)₂ in references. **Table 1** indicates that BET specific surface areas of the α -Ni(OH)₂-MS are higher than those of the Ni(OH)₂ products.

The electrocatalytic performances of α -Ni(OH)₂-MS and α -Ni(OH)₂-EG toward OER were investigated in 1M KOH electrolyte by a standard three-electrode method. For comparison, bare NF was also tested under the same condition. **Figure 6A** shows the LSV curves at a scanning rates of 5 mV s⁻¹ in the potential range of 0–0.8 V. The oxidation peaks around 1.37 eV (prior to onset of OER) observed for the Ni(OH)₂-based electrodes could be ascribed to the transformation of Ni (II) to Ni (III) species (Tong et al., 2012). At a current density of 10 mA cm², the overpotential for the α -Ni(OH)₂-MS is 320 mV, while the overpotential for the α -Ni(OH)₂-EG and bare NF are 350 and 420 mV, respectively. In order to gain more insight into the catalytic activity, the LSV curves were also converted into Tafel plots, as shown in **Figure 6B**, in which

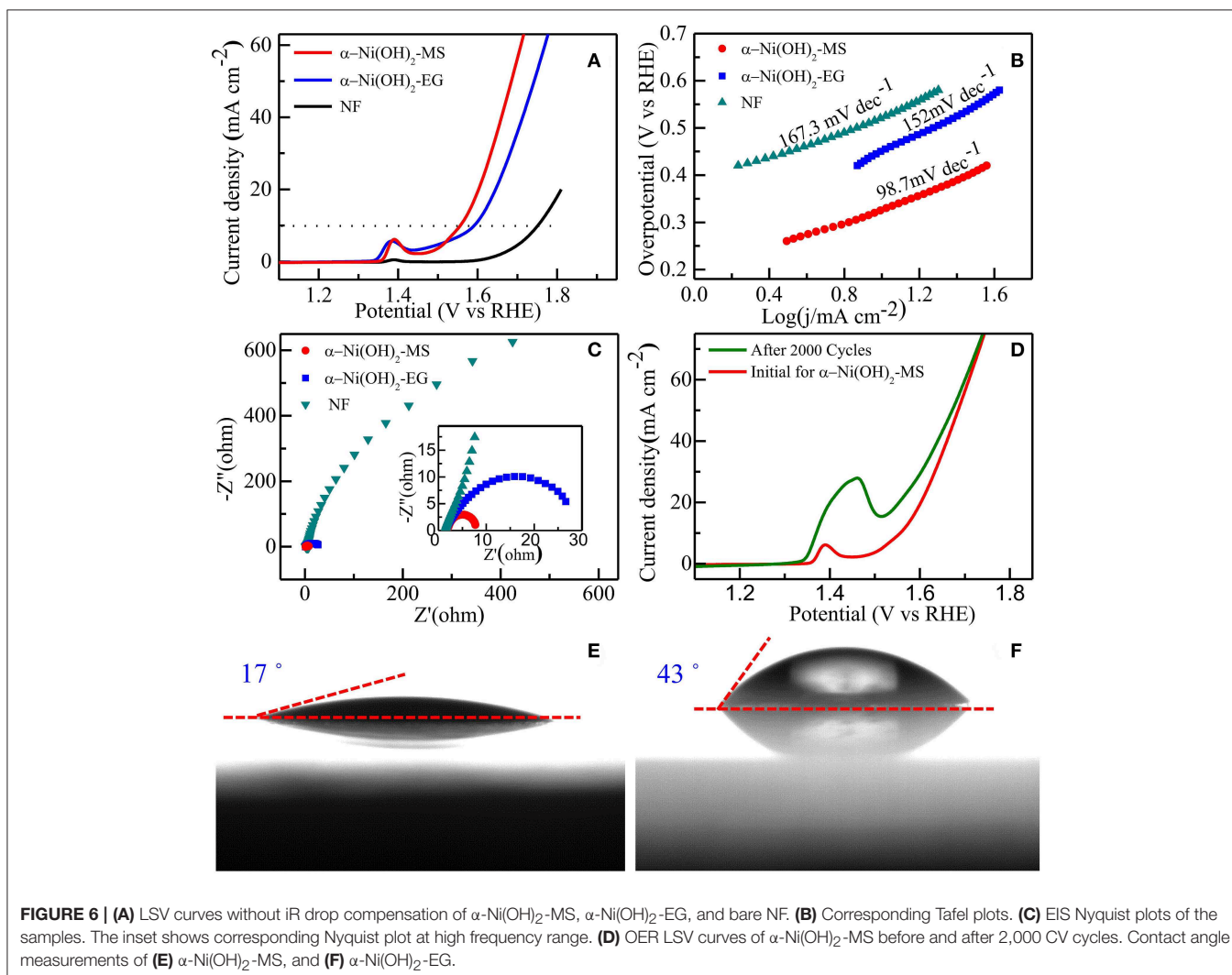


TABLE 2 | Comparison of OER performance of the most typical mono- and bi-metal hydroxide catalysts in alkaline electrolyte.

Materials	Electrolyte	Mass loading (mg cm ⁻²)	η_{10} (mV)	Tafel slope (mV dec ⁻¹)	Ref.
α -Ni(OH) ₂ -MS	1.0 M KOH	0.30	320	98.7	This work
α -Ni(OH) ₂ nanosheets	1.0 M KOH	0.16	350	144	Liu et al., 2015
α -Ni(OH) ₂ hollow spheres	0.1 M KOH	0.20	330	42	Xu et al., 2008
α -Ni(OH) ₂ -NP	1.0 M KOH	0.20	260	78.6	Luan et al., 2018
α -Ni(OH) ₂ -NB	1.0 M KOH	0.20	320	92.4	Luan et al., 2018
α -Ni(OH) ₂ /NF	1.0 M KOH	0.80	340	105	Wu et al., 2018
α -Ni(OH) ₂ /NF	1.0 M KOH	–	400	161.8	Liu et al., 2018
α -Ni(OH) ₂ spheres	0.1 M KOH	0.20	331	42	Gao et al., 2014
β -Ni(OH) ₂ hexagonal NPs	0.1 M KOH	0.20	444	111	Gao et al., 2014
β -Ni(OH) ₂ NPs	1.0 M KOH	0.14	331	47	Stern et al., 2015
β -Ni(OH) ₂ nanoplate/MCNT	0.1 M KOH	0.28	474	87	Zhou et al., 2014
α -Co(OH) ₂ nanosheets	1.0 M KOH	0.32	388	107	Zhang et al., 2018
NiCo LDH/carbon paper	1.0 M KOH	0.23	367	40	Liang et al., 2015
NiMn LDH	1.0 M KOH	–	385	80	Wang Y. et al., 2018

the overpotential is plotted as a function of the current density logarithm. As we know, the Tafel slope is an important parameter to evaluate the evolution of OER kinetics. The Tafel slope of the α -Ni(OH)₂-MS is 98.7 mV dec⁻¹, which is smaller than that of α -Ni(OH)₂-EG (152 mV dec⁻¹) and bare NF (167.3 mV dec⁻¹). The smaller Tafel slope of the α -Ni(OH)₂-MS implies the fast electron and mass transfer between the catalyst and the electrolyte during the water oxidation process. This indicates that the α -Ni(OH)₂-MS is an efficient catalyst toward OER. To further verify the electrode kinetics, the electrochemical impedance spectroscopy (EIS) technique was carried out by using a perturbation amplitude of 5 mV in the frequency range between 0.01 Hz and 100 kHz, as shown in **Figure 6C**. Compared to the bare NF, the α -Ni(OH)₂-MS and α -Ni(OH)₂-EG exhibit a quasi-semicircle. The smaller semicircle diameter of α -Ni(OH)₂-MS indicates this sample has a lower charge transfer resistance (R_{ct}), which is mainly due to the synergistic effect of the large contact areas with electrolyte and the short ion diffusion distance resulting from their unique hierarchical microstructures. In our case, the interconnected ultrathin nanosheets structure leads to the formation of a percolated conductive network, and this can facilitate charge separation. Stability is another important factor for evaluating electrocatalysts. The LSV curves of α -Ni(OH)₂-MS before and after 2,000 cycles are shown in **Figure 6D**. Interestingly, the OER activity after 2,000 cycles is found to increase. Such enhanced kinetics after 2,000 cycles may be ascribed to the formation of a more active γ -NiOOH phase, and subsequently, to increased electron conductivity of the electrodes (Oliva et al., 1982; Medway et al., 2006; Bediako et al., 2013; Gao et al., 2014). The electrochemical stability of the α -Ni(OH)₂-MS was further characterized by the chronoamperometric ($i-t$) response measurement. As shown in **Figure S6**, under continuous testing at a static potential (1.55 V vs. RHE), the current density increases at first and reaches a stable value, which is consistent with the LSV curves before and after 2,000 cycles mentioned above. Then, the current density remains stable after a long period of the OER tests, showing an

excellent stability under alkaline conditions. In addition, we also checked the static angles of the α -Ni(OH)₂-MS and α -Ni(OH)₂-EG, as shown in **Figures 6E,F**. The static contact angle is 17° for α -Ni(OH)₂-MS, which is smaller than that of α -Ni(OH)₂-EG (43°). Therefore, the α -Ni(OH)₂-MS possess a much more hydrophilic surface. The better catalyst surface wettability would accelerate the electrolyte penetration, and facilitate the migration of hydroxyl groups and oxygen generation as well (Zhou et al., 2018).

Here, the α -Ni(OH)₂-MS possesses sufficient exposed active sites and OER-favored adsorption/diffusion properties as mentioned above. What's more, the stable hierarchical structure can avoid the aggregation of the nanosheets. To our knowledge, the α -Ni(OH)₂-MS demonstrates the better OER activity than that of most monometal hydroxide. It also outperforms many bimetal hydroxide OER catalysts, in which the synergistic effects improve their OER activity. For comparison, we listed the results in **Table 2**. These results not only exhibit the superiority of the α -Ni(OH)₂-MS, but also provide a good example and synthesis method to construct efficient OER catalysts.

CONCLUSIONS

In summary, the monodispersed α -Ni(OH)₂ microspheres assembled by ultrathin nanosheets were successfully synthesized by a facile and surfactant-free solvothermal method. The BET specific surface area of the α -Ni(OH)₂-MS architectures reached 169.94 m²g⁻¹. The electrocatalytic performances of the sample toward OER were investigated in 1M KOH electrolyte by a standard three-electrode system. At a current density of 10 mA cm², the overpotential for the α -Ni(OH)₂-MS is 320 mV with a Tafel slope of 98.7 mV dec⁻¹. The EIS measurement indicates that this sample has a lower charge transfer resistance. The results indicate that the synthesized α -Ni(OH)₂-MS possesses sufficient exposed active sites and OER-favored adsorption/diffusion properties. The unique hierarchical structure can avoid the

aggregation of the nanosheets. Therefore, this work provides a meaningful approach for the synthesis of efficient OER catalysts.

DATA AVAILABILITY

The raw data supporting the conclusions of this manuscript will be made available by the authors, without undue reservation, to any qualified researcher.

AUTHOR CONTRIBUTIONS

JY: article writing, synthesis of material, electrochemical test. SP: electrochemical test, SEM. YZ: electrochemical data analysis. QL: XRD and XPS data analysis. BL: the overall design.

REFERENCES

- Aghazadeh, M., Ghaemi, M., Sabour, B., and Dalvand, S. (2014). Electrochemical preparation of α -Ni(OH)₂ ultrafine nanoparticles for high-performance supercapacitors. *J. Solid State Electrochem.* 18, 1569–1584. doi: 10.1007/s10008-014-2381-7
- Aghazadeh, M., Golikand, A. N., and Ghaemi, M. (2011). Synthesis, characterization, and electrochemical properties of ultrafine β -Ni(OH)₂ nanoparticles. *Int. Hydrogen Energy J.* 36, 8674–8679. doi: 10.1016/j.ijhydene.2011.03.144
- Alarawi, A., Ramalingam, V., and He, J.-H. (2019). Recent advances in emerging single atom confined two-dimensional materials for water splitting applications. *Materials Today Energy* 11, 1–23. doi: 10.1016/j.mtener.2018.10.014
- Anantharaj, S., Ede, S. R., Sakthikumar, K., Karthick, K., Mishra, S., and Kundu, S. (2016). Recent trends and perspectives in electrochemical water splitting with an emphasis on sulfide, selenide, and phosphide catalysts of Fe, Co, and Ni: a review. *ACS Catalysis* 6, 8069–8097. doi: 10.1021/acscatal.6b02479
- Anantharaj, S., Karthik, P. E., and Kundu, S. (2017). Petal-like hierarchical array of ultrathin Ni(OH)₂ nanosheets decorated with Ni(OH)₂ nanoburrs: a highly efficient OER electrocatalyst. *Catal. Sci. Technol.* 7, 882–893. doi: 10.1039/C6CY02282K
- Bediako, D. K., Surendranath, Y., and Nocera, D. G. (2013). Mechanistic studies of the oxygen evolution reaction mediated by a nickel-borate thin film electrocatalyst. *J. Am. Chem. Soc.* 135, 3662–3674. doi: 10.1021/ja3126432
- Chen, S., Mi, J.-L., Zhang, P., Feng, Y.-H., Yong, Y. C., and Shi, W.-D. (2018). Control synthesis of nickel selenides and their multiwalled carbon nanotubes composites as electrocatalysts for enhanced water oxidation. *J. Phys. Chem. C* 122, 26096–26104. doi: 10.1021/acs.jpcc.8b09259
- Cheng, M.-Y., and Hwang, B.-J. (2009). Control of uniform nanostructured α -Ni(OH)₂ with self-assembly sodium dodecyl sulfate templates. *J. Colloid Interface Sci.* 337, 265–271. doi: 10.1016/j.jcis.2009.05.008
- Cordoba, S. I., Carbonio, R. E., Teijelo, M. L., and Macagno, V. A. (1986). The electrochemical response of binary mixtures of hydrous transition metal hydroxides co-precipitated on conducting substrates with reference to the oxygen evolution reaction. *Electrochim. Acta* 31, 1321–1332. doi: 10.1016/0013-4686(86)80155-4
- Dong, B., Zhao, X. G., Han, Q., Li, X., Shang, X., Liu, Y.-R., et al. (2016). Two-step synthesis of binary Ni-Fe sulfides supported on nickel foam as highly efficient electrocatalysts for the oxygen evolution reaction. *J. Mater. Chem. A* 4, 13499–13508. doi: 10.1039/C6TA03177C
- Dou, Y., Liao, T., Ma, Z., Tian, D., Liu, Q., Xiao, F., et al. (2016). Graphene-like holey Co₃O₄ nanosheets as a highly efficient catalyst for oxygen evolution reaction. *Nano Energy* 30, 267–275. doi: 10.1016/j.nanoen.2016.10.020

FUNDING

This work was supported by the Natural Science Foundation of Anhui Province (Grant Nos. 1608085QE90, 1708085ME96), Talent Support Program of Anhui Province (Grant No. gxgwx2018083), Natural Science Foundation of China (Grant Nos. 11504120, 51302102), Natural Science Foundation of Anhui Higher Education Institutions of China (Grant No. KJ2015A095).

SUPPLEMENTARY MATERIAL

The Supplementary Material for this article can be found online at: <https://www.frontiersin.org/articles/10.3389/fmats.2019.00124/full#supplementary-material>

- Du, H., Wang, Y., Yuan, H., and Jiao, L. (2016). Facile synthesis and high capacitive performance of 3D hierarchical Ni(OH)₂ microspheres. *Electrochim. Acta* 196, 84–91. doi: 10.1016/j.electacta.2016.02.190
- Du, J., Yang, M., Zhang, F., Cheng, X., Wu, H., Qin, H., et al. (2018). Enhanced charge separation of CuS and CdS quantum-dot-cosensitized porous TiO₂-based photoanodes for photoelectrochemical water splitting. *Ceram. Int.* 44, 3099–3106. doi: 10.1016/j.ceramint.2017.11.075
- Du, P., and Eisenberg, R. (2012). Catalysts made of earth-abundant elements (Co, Ni, Fe) for water splitting: recent progress and future challenges. *Energy Environ. Sci.* 5, 6012–6021. doi: 10.1039/c2ee03250c
- Gao, M., Sheng, W., Zhuang, Z., Fang, Q., Gu, S., Jiang, J., et al. (2014). Efficient water oxidation using nanostructured α -nickel-hydroxide as an electrocatalyst. *J. Am. Chem. Soc.* 136, 7077–7084. doi: 10.1021/ja502128j
- Gong, M., and Dai, H. (2015). A mini review of NiFe-based materials as highly active oxygen evolution reaction electrocatalysts. *Nano Res.* 8, 23–39. doi: 10.1007/s12274-014-0591-z
- Gong, M., Li, Y., Wang, H., Liang, Y., Wu, J. Z., Zhou, J., et al. (2013). An advanced Ni-Fe layered double hydroxide electrocatalyst for water oxidation. *J. Am. Chem. Soc.* 135, 8452–8455. doi: 10.1021/ja4027715
- Guo, P., Wu, Y.-X., Lau, W.-M., Liu, H., and Liu, L.-M. (2017). CoS nanosheet arrays grown on nickel foam as an excellent OER catalyst. *J. Alloys Compd.* 723, 772–778. doi: 10.1016/j.jallcom.2017.06.299
- Jeevanandam, P., Koltypin, Y., and Gedanken, A. (2001). Synthesis of nanosized α -nickel hydroxide by a sonochemical method. *Nano Lett.* 1, 263–266. doi: 10.1021/nl010003p
- Jia, Y., Zhang, L., Gao, G., Chen, H., Wang, B., Zhou, J., et al. (2017). A heterostructure coupling of exfoliated Ni-Fe hydroxide nanosheet and defective graphene as a bifunctional electrocatalyst for overall water splitting. *Adv. Mater.* 29:1700017. doi: 10.1002/adma.201700017
- Kadi, M. W., and Mohamed, R. M. (2019). Increasing visible light water splitting efficiency through synthesis route and charge separation in mesoporous g-C₃N₄ decorated with WO₃ nanoparticles. *Ceram. Int.* 45, 3886–3893. doi: 10.1016/j.ceramint.2018.11.061
- Kim, B. N., Seo, G. K., Hwang, S. W., Yu, H., Ahn, B., Seo, H., et al. (2018). Photophysical properties and photoelectrochemical performances of sol-gel derived copper stannate (CuSnO₃) amorphous semiconductor for solar water splitting application. *Ceram. Int.* 44, 1843–1849. doi: 10.1016/j.ceramint.2017.10.119
- Krehula, S., Ristić, M., Wu, C., Li, X., Jiang, L., Wang, J., et al. (2018). Influence of Fe(III) doping on the crystal structure and properties of hydrothermally prepared β -Ni(OH)₂ nanostructures. *J. Alloys Compd.* 750, 687–695. doi: 10.1016/j.jallcom.2018.04.032
- Lee, J. W., Ahn, T., Kim, J. H., Ko, J. M., and Kim, J.-D. (2011a). Nanosheets based mesoporous NiO microspherical structures via facile and template-free method for high performance supercapacitors. *Electrochim. Acta* 56, 4849–4857. doi: 10.1016/j.electacta.2011.02.116

- Lee, J. W., Ko, J. M., and Kim, J.-D. (2011b). Hierarchical microspheres based on α -Ni(OH)₂ nanosheets intercalated with different anions: synthesis, anion exchange, and effect of intercalated anions on electrochemical capacitance. *J. Phys. Chem. C* 115, 19445–19454. doi: 10.1021/jp206379h
- Li, B. Q., Zhang, S. Y., Tang, C., Cui, X., and Zhang, Q. (2017). Anionic regulated NiFe (Oxy)sulfide electrocatalysts for water oxidation. *Small* 13:1700610. doi: 10.1002/smll.201700610
- Li, P., Lv, F., Xu, Z., Qi, G., and Zhang, Y. (2013). Functions of surfactants in the one-step synthesis of surfactant-intercalated LDHs. *J. Mater. Sci.* 48, 5437–5446. doi: 10.1007/s10853-013-7337-2
- Li, S., Wang, Y., Peng, S., Zhang, L., Al-Enizi, A. M., Zhang, H., et al. (2016). Co-Ni-based nanotubes/nanosheets as efficient water splitting electrocatalysts. *Adv. Energy Mater.* 6:1501661. doi: 10.1002/aenm.201501661
- Liang, H., Meng, F., Cabán-Acevedo, M., Li, L., Forticaux, A., Xiu, L., et al. (2015). Hydrothermal continuous flow synthesis and exfoliation of NiCo layered double hydroxide nanosheets for enhanced oxygen evolution catalysis. *Nano Lett.* 15, 1421–1427. doi: 10.1021/nl504872s
- Liu, G., Sun, Z., Zhang, X., Wang, H., Wang, G., Wu, X., et al. (2018). Vapor-phase hydrothermal transformation of a nanosheet array structure Ni(OH)₂ into ultrathin Ni₃S₂ nanosheets on nickel foam for high-efficiency overall water splitting. *J. Mater. Chem. A* 6, 19201–19209. doi: 10.1039/C8TA07162D
- Liu, W., Bao, J., Guan, M., Zhao, Y., Lian, J., Qiu, J., et al. (2017). Nickel-cobalt-layered double hydroxide nanosheet arrays on Ni foam as a bifunctional electrocatalyst for overall water splitting. *Dalton Trans.* 46, 8372–8376. doi: 10.1039/C7DT00906B
- Liu, X., Liu, W., Ko, M., Park, M., Kim, M. G., Oh, P., et al. (2015). Metal (Ni, Co)-metal oxides/graphene nanocomposites as multifunctional electrocatalysts. *Adv. Funct. Mater.* 25, 5799–5808. doi: 10.1002/adfm.201502217
- Liu, Z., Ma, R., Osada, M., Takada, K., and Sasaki, T. (2005). Selective and controlled synthesis of α - and β -cobalt hydroxides in highly developed hexagonal platelets. *J. Am. Chem. Soc.* 127, 13869–13874. doi: 10.1021/ja0523338
- Liu, Z., Yuan, C., and Teng, F. (2019). Crystal facets-predominated oxygen evolution reaction activity of earth abundant CoMoO₄ electrocatalyst. *J. Alloys Compd.* 781, 460–466. doi: 10.1016/j.jallcom.2018.12.026
- Luan, C., Liu, G., Liu, Y., Yu, L., Wang, Y., Xiao, Y., et al. (2018). Structure effects of 2D materials on α -nickel hydroxide for oxygen evolution reaction. *ACS Nano* 12, 3875–3885. doi: 10.1021/acsnano.8b01296
- Ma, W., Ma, R., Wang, C., Liang, J., Liu, X., Zhou, K., et al. (2015). A superlattice of alternately stacked Ni-Fe hydroxide nanosheets and graphene for efficient splitting of water. *ACS Nano* 9, 1977–1984. doi: 10.1021/nn5069836
- Man, I. C., Su, H.-Y., Calle-Vallejo, F., Hansen, H. A., Martínez, J. I., Inoglu, N. G., et al. (2011). Universality in oxygen evolution electrocatalysis on oxide surfaces. *ChemCatChem* 3, 1159–1165. doi: 10.1002/cctc.201000397
- Masa, J., Weide, P., Peeters, D., Sinev, I., Xia, W., Sun, Z., et al. (2016). Amorphous cobalt boride (Co₂B) as a highly efficient nonprecious catalyst for electrochemical water splitting: oxygen and hydrogen evolution. *Adv. Energy Mater.* 6:1502313. doi: 10.1002/aenm.201502313
- McCrorry, C. C., Jung, S., Ferrer, I. M., Chatman, S. M., Peters, J. C., and Jaramillo TF. (2015). Benchmarking hydrogen evolving reaction and oxygen evolving reaction electrocatalysts for solar water splitting devices. *J. Am. Chem. Soc.* 137, 4347–4357. doi: 10.1021/ja510442p
- McCrorry, C. C., Jung, S., Peters, J. C., and Jaramillo, T. F. (2013). Benchmarking heterogeneous electrocatalysts for the oxygen evolution reaction. *J. Am. Chem. Soc.* 135, 16977–16987. doi: 10.1021/ja407115p
- Medway, S. L., Lucas, C. A., Kowal, A., Nichols, R. J., and Johnson, D. (2006). *In situ* studies of the oxidation of nickel electrodes in alkaline solution. *J. Electroanal. Chem.* 587, 172–181. doi: 10.1016/j.jelechem.2005.11.013
- Menezes, P. W., Indra, A., Levy, O., Kailasam, K., Gutkin, V., Pfrommer, J., et al. (2015). Using nickel manganese oxide catalysts for efficient water oxidation. *Chem. Commun.* 51, 5005–5008. doi: 10.1039/C4CC09671A
- Midilli, A., and Dincer, I. (2008). Hydrogen as a renewable and sustainable solution in reducing global fossil fuel consumption. *Int. Hydrogen Energy J.* 33, 4209–4222. doi: 10.1016/j.ijhydene.2008.05.024
- Niu, S., Jiang, W.-J., Tang, T., Zhang, Y., Li, J.H., and Hu, J.S. (2017). Facile and scalable synthesis of robust Ni(OH)₂ nanoplate arrays on NiAl foil as hierarchical active scaffold for highly efficient overall water splitting. *Adv. Sci.* 4:1700084. doi: 10.1002/advs.201700084
- Oliva, P., Leonardi, J., Laurent, J. F., Delmas, C., Braconnier, J. J., Figlarz, M., et al. (1982). Review of the structure and the electrochemistry of nickel hydroxides and oxy-hydroxides. *J. Power Sources* 8, 229–255. doi: 10.1016/0378-7753(82)80057-8
- Ouyang, C., Wang, X., Wang, C., Zhang, X., Wu, J., Ma, Z., et al. (2015). Hierarchically porous Ni₃S₂ nanorod array foam as highly efficient electrocatalyst for hydrogen evolution reaction and oxygen evolution reaction. *Electrochim. Acta* 174, 297–301. doi: 10.1016/j.electacta.2015.05.186
- Peng, Z., Jia, D., Al-Enizi, A. M., Elzatahy, A. A., and Zheng, G. (2015). From water oxidation to reduction: homologous Ni-Co based nanowires as complementary water splitting electrocatalysts. *Adv. Energy Materials* 5:1402031. doi: 10.1002/aenm.201402031
- Petrykin, V., Macounova, K., Shlyakhtin, O. A., and Krtil, P. (2010). Tailoring the selectivity for electrocatalytic oxygen evolution on ruthenium oxides by zinc substitution. *Angew. Chem.* 122, 4923–4925. doi: 10.1002/ange.200907128
- Qi, J., Zhang, W., Xiang, R., Liu, K., Wang, H.Y., Chen, M., et al. (2015). Porous nickel-iron oxide as a highly efficient electrocatalyst for oxygen evolution reaction. *Adv. Sci.* 2:1500199. doi: 10.1002/advs.201500199
- Qiu, Y., Xin, L., and Li, W. (2014). Electrocatalytic oxygen evolution over supported small amorphous Ni-Fe nanoparticles in alkaline electrolyte. *Langmuir* 30, 7893–7901. doi: 10.1021/la501246e
- Rakov, D., Li, Y., Niu, S., and Xu, P. (2018). Insight into Mn and Ni doping of Ni_{1-x}Mn_xPS₃ and Mn_{1-x}Ni_xPS₃ nanosheets on electrocatalytic hydrogen and oxygen evolution activity. *J. Alloys Compd.* 769, 532–538. doi: 10.1016/j.jallcom.2018.08.041
- Reier, T., Oezaslan, M., and Strasser, P. (2012). Electrocatalytic Oxygen Evolution Reaction (OER) on Ru, Ir, and Pt catalysts: a comparative study of nanoparticles and bulk materials. *ACS Catalysis* 2, 1765–1772. doi: 10.1021/cs3003098
- Roger, I., Shipman, M. A., and Symes, M. D. (2017). Earth-abundant catalysts for electrochemical and photoelectrochemical water splitting. *Nat. Rev. Chem.* 1:0003. doi: 10.1038/s41570-016-0003
- Shi, Y., and Zhang, B. (2016). Recent advances in transition metal phosphide nanomaterials: synthesis and applications in hydrogen evolution reaction. *Chem. Soc. Rev.* 45, 1529–1541. doi: 10.1039/C5CS00434A
- Stern, L.-A., Feng, L., Song, F., and Hu, X. (2015). Ni₂P as a Janus catalyst for water splitting: the oxygen evolution activity of Ni₂P nanoparticles. *Energy Environ. Sci.* 8, 2347–2351. doi: 10.1039/C5EE01155H
- Stern, L.-A., and Hu, X. (2014). Enhanced oxygen evolution activity by NiO_x and Ni(OH)₂ nanoparticles. *Faraday Discuss.* 176, 363–379. doi: 10.1039/C4FD00120F
- Subbaraman, R., Tripkovic, D., Chang, K.C., Strmcnik, D., Paulikas, A. P., Hirusit, P., et al. (2012). Trends in activity for the water electrolyser reactions on 3d M(Ni,Co,Fe,Mn) hydr(oxy)oxide catalysts. *Nat. Mater.* 11:550. doi: 10.1038/nmat3313
- Suen, N. T., Hung, S. F., Quan, Q., Zhang, N., Xu, Y. J., and Chen, H. M. (2017). Electrocatalysis for the oxygen evolution reaction: recent development and future perspectives. *Chem. Soc. Rev.* 46, 337–365. doi: 10.1039/C6CS00328A
- Sumboja, A., Chen, J., Zong, Y., Lee, P. S., and Liu, Z. (2017). NiMn layered double hydroxides as efficient electrocatalysts for the oxygen evolution reaction and their application in rechargeable Zn-air batteries. *Nanoscale* 9, 774–780. doi: 10.1039/C6NR08870H
- Sun, S., Zhang, Y.-C., Shen, G., Wang, Y., Liu, X., Duan, Z., et al. (2019). Photoinduced composite of Pt decorated Ni(OH)₂ as strongly synergetic cocatalyst to boost H₂O activation for photocatalytic overall water splitting. *Appl. Catalysis B Environ.* 243, 253–261. doi: 10.1016/j.apcatb.2018.10.051
- Tahir, M., Pan, L., Idrees, F., Zhang, X., Wang, L., Zou, J.-J., et al. (2017). Electrocatalytic oxygen evolution reaction for energy conversion and storage: a comprehensive review. *Nano Energy* 37, 136–157. doi: 10.1016/j.nanoen.2017.05.022
- Tian, X., Cheng, C., Qian, L., Zheng, B., Yuan, H., Xie, S., et al. (2012). Microwave-assisted non-aqueous homogenous precipitation of nanoball-like mesoporous α -Ni(OH)₂ as a precursor for NiO_x and its application as a pseudocapacitor. *J. Mater. Chem.* 22, 8029–8035. doi: 10.1039/c2jm16057a
- Tong, G.-X., Liu, F.-T., Wu, W.-H., Shen, J.-P., Hu, X., and Liang, Y. (2012). Polymorphous α - and β -Ni(OH)₂ complex architectures: morphological and phasal evolution mechanisms and enhanced catalytic activity as non-enzymatic glucose sensors. *CrystEngComm* 14, 5963–5973. doi: 10.1039/c2ce25622c

- Wang, D., Guan, B., Li, Y., Li, D., Xu, Z., Hu, Y. et al. (2018). Morphology-controlled synthesis of hierarchical mesoporous α -Ni(OH)₂ microspheres for high-performance asymmetric supercapacitors. *J. Alloys Compd.* 737, 238–247. doi: 10.1016/j.jallcom.2017.12.095
- Wang, H.-Y., Hsu, Y.-Y., Chen, R., Chan, T.-S., Chen, H. M., and Liu, B. (2015). Ni³⁺-induced formation of active NiOOH on the spinel Ni-Co oxide surface for efficient oxygen evolution reaction. *Adv. Energy Mater.* 5:1500091. doi: 10.1002/aenm.201500091
- Wang, J., Cui, W., Liu, Q., Xing, Z., Asiri, A. M., and Sun, X. (2016). Recent progress in cobalt-based heterogeneous catalysts for electrochemical water splitting. *Adv. Mater.* 28, 215–230. doi: 10.1002/adma.201502696
- Wang, M., Lai, Y., Fang, J., Qin, F., Zhang, Z., Li, J., et al. (2016). Hydrangea-like NiCo₂S₄ hollow microspheres as an advanced bifunctional electrocatalyst for aqueous metal/air batteries. *Catal. Sci. Technol.* 6, 434–437. doi: 10.1039/C5CY01656H
- Wang, Q., Liu, S., Sun, H., and Lu, Q. (2015). Synthesis of a flower-like Co-doped Ni(OH)₂ composite for high-performance supercapacitors. *RSC Adv.* 5, 48181–48186. doi: 10.1039/C5RA03774C
- Wang, S., He, P., Jia, L., He, M., Zhang, T., Dong, F., et al. (2019). Nanocoral-like composite of nickel selenide nanoparticles anchored on two-dimensional multi-layered graphitic carbon nitride: a highly efficient electrocatalyst for oxygen evolution reaction. *Appl. Catal. B Environ.* 243, 463–469. doi: 10.1016/j.apcatb.2018.10.071
- Wang, Y., Liu, X., Zhang, N., Qiu, G., and Ma, R. (2018). Cobalt-doped Ni-Mn layered double hydroxide nanoplates as high-performance electrocatalyst for oxygen evolution reaction. *Appl. Clay Sci.* 165, 277–283. doi: 10.1016/j.clay.2018.07.036
- Wu, J., Subramaniam, J., Liu, Y., Geng, D., and Meng, X. (2018). Facile assembly of Ni(OH)₂ nanosheets on nitrogen-doped carbon nanotubes network as high-performance electrocatalyst for oxygen evolution reaction. *J. Alloys Compd.* 731, 766–773. doi: 10.1016/j.jallcom.2017.10.096
- Xie, J., Yang, C., Duan, M., Tang, J., Wang, Y., Wang, H., et al. (2018). Amorphous NiP as cocatalyst for photocatalytic water splitting. *Ceram. Int.* 44, 5459–5465. doi: 10.1016/j.ceramint.2017.12.179
- Xu, L., Ding, Y.-S., Chen, C.-H., Zhao, L., Rimkus, C., Joesten, R., et al. (2008). 3D Flowerlike α -nickel hydroxide with enhanced electrochemical activity synthesized by microwave-assisted hydrothermal method. *Chem. Mater.* 20, 308–316. doi: 10.1021/cm702207w
- Yan, J., Fan, Z., Sun, W., Ning, G., Wei, T., Zhang, Q., et al. (2012). Advanced asymmetric supercapacitors based on Ni(OH)₂/graphene and porous graphene electrodes with high energy density. *Adv. Funct. Mater.* 22, 2632–2641. doi: 10.1002/adfm.201102839
- Yan, K.-L., Shang, X., Li, Z., Dong, B., Li, X., Gao, W.-K., et al. (2017). Ternary mixed metal Fe-doped NiCo₂O₄ nanowires as efficient electrocatalysts for oxygen evolution reaction. *Appl. Surf. Sci.* 416, 371–378. doi: 10.1016/j.apsusc.2017.04.204
- Yang, H., Zhang, Y., Hu, F., and Wang, Q. (2015). Urchin-like CoP nanocrystals as hydrogen evolution reaction and oxygen reduction reaction dual-electrocatalyst with superior stability. *Nano Lett.* 15, 7616–7620. doi: 10.1021/acs.nanolett.5b03446
- Yu, X., Zhang, M., Yuan, W., and Shi, G. (2015). A high-performance three-dimensional Ni-Fe layered double hydroxide/graphene electrode for water oxidation. *J. Mater. Chem. A* 3, 6921–6928. doi: 10.1039/C5TA01034A
- Zhai, Z., Liu, Q., Zhu, Y., Cao, J., and Shi, S. (2019). Synthesis of Ni(OH)₂/graphene composite with enhanced electrochemical property by stirring solvothermal method. *J. Alloys Compd.* 775, 1316–1323. doi: 10.1016/j.jallcom.2018.10.262
- Zhang, B., Zhang, J., Tan, X., Tan, D., Shi, J., Zhang, F., et al. (2018). One-step synthesis of ultrathin α -Co(OH)₂ nanomeshes and their high electrocatalytic activity toward the oxygen evolution reaction. *Chem. Commun.* 54, 4045–4048. doi: 10.1039/C8CC01724G
- Zhao, Z., Wu, H., He, H., Xu, X., and Jin, Y. (2014). A high-performance binary Ni-Co hydroxide-based water oxidation electrode with three-dimensional coaxial nanotube array structure. *Adv. Funct. Mater.* 24, 4698–4705. doi: 10.1002/adfm.201400118
- Zhou, Q., Chen, Y., Zhao, G., Lin, Y., Yu, Z., Xu, X., et al. (2018). Active-site-enriched iron-doped nickel/cobalt hydroxide nanosheets for enhanced oxygen evolution reaction. *ACS Catalysis* 8, 5382–5390. doi: 10.1021/acscatal.8b01332
- Zhou, X., Xia, Z., Zhang, Z., Ma, Y., and Qu, Y. (2014). One-step synthesis of multi-walled carbon nanotubes/ultra-thin Ni(OH)₂ nanoplate composite as efficient catalysts for water oxidation. *J. Mater. Chem. A*, 2, 11799–11806. doi: 10.1039/C4TA01952K

Conflict of Interest Statement: The authors declare that the research was conducted in the absence of any commercial or financial relationships that could be construed as a potential conflict of interest.

Copyright © 2019 Yu, Pan, Zhang, Liu and Li. This is an open-access article distributed under the terms of the Creative Commons Attribution License (CC BY). The use, distribution or reproduction in other forums is permitted, provided the original author(s) and the copyright owner(s) are credited and that the original publication in this journal is cited, in accordance with accepted academic practice. No use, distribution or reproduction is permitted which does not comply with these terms.